*J. Numer. Math.*, Vol. 0, No. 0, pp. 1–23 (2004)
 *Prepared using* jnm.sty *[Version: 02.02.2002 v1.2]*

# Analysis and simulation of a coupled hyperbolic/parabolic model problem

J.-P. Croisille,* A. Ern,† T. Lelièvre,† and J. Proft†‡

*Received* *Communicated by A. Quarteroni*

**Abstract** — We investigate a periodic one-dimensional degenerate advection-diffusion equation. The problem is hyperbolic in a subinterval and parabolic in the complement, and the boundary conditions only impose the periodicity of the advective-diffusive flux to ensure mass conservation. Following Gastaldi and Quarteroni (1989), an additional condition is enforced to select the "physically acceptable" solution as the limit of vanishing viscosity solutions, namely the continuity of the solution at the parabolic to hyperbolic interface. Using this condition, we establish the well-posedness of the Cauchy problem in the framework of the evolution linear semi-groups theory. We also discuss the regularity of the solution when the initial condition is too rough to be in the domain of the evolution operator. Then, we present a suite of reference solutions for various sets of data. This solutions can be used to assess the robustness of numerical schemes. In particular, we present results obtained with a simple upwind scheme, a finite volume box-scheme, and the local discontinuous Galerkin method. The three schemes select automatically the physically acceptable solution, the latter two offering a much sharper resolution of the solution profiles.

**Keywords:** Hyperbolic/parabolic, interface conditions, semigroup theory, finite elements, finite volumes, box-schemes

## 1. INTRODUCTION

The main motivation for this work is to analyze the advection-diffusion of a scalar variable $u(t,x)$ in a medium having strong heterogeneities. Our aim is to address an evolution problem that changes spatially its mathematical character, namely hyperbolic in some parts of the domain and parabolic in the other parts. The model evolving $u(t,x)$ is an advection-diffusion equation in the form

$$\partial_t u + \partial_x \mathscr{F}(x,u,\partial_x u) = f, \tag{1.1}$$

with source term $f$ and the flux

$$\mathscr{F}(x,u,\partial_x u) = \beta u - \alpha(x)\partial_x u. \tag{1.2}$$

*Laboratoire de Mathématiques, Université de Metz, Ile du Saulcy, F-57045 Metz cedex, France

†CERMICS, Ecole nationale des ponts et chaussées, 6/8 avenue Blaise Pascal, Champs sur Marne, F-77455 Marne-la-Vallée cedex 2, France

‡LAMA, CNRS UMR 8050, Université Marne-la-Vallée, Champs sur Marne, F-77454 Marne-la-Vallée cedex 2, France

This work was supported by CNRS and GdR MOMAS

In (1.1)–(1.2), the advection velocity $\beta$ is solenoidal. The diffusion coefficient $\alpha(x)$ allows to switch between a purely advective equation ($\alpha(x) = 0$) and an advection-diffusion equation ($\alpha(x) > 0$). In applications, the variable $u(t,x)$ can mimic for instance any type of pollutant concentration in geological layers.

As a model problem, we investigate a 2-periodic setting in one space dimension. Let $\Omega = (0,2)$, $\Omega_P = (0,1)$, and $\Omega_H = (1,2)$. The advection velocity is taken constant equal to 1; the diffusion coefficient is given by $\alpha(x) = \alpha_0 > 0$ for $x \in \Omega_P$ (the parabolic zone) and $\alpha(x) = 0$ for $x \in \Omega_H$ (the hyperbolic zone). We investigate the following Cauchy problem:

$$\begin{cases} \partial_t u + \partial_x \mathscr{F}(x,u,\partial_x u) = f & x \in \Omega,\ t > 0, \\ u(t=0,\cdot) = u_0 & x \in \Omega, \end{cases} \tag{1.3}$$

with advective-diffusive flux

$$\mathscr{F}(x,u,\partial_x u) = \begin{cases} u - \alpha_0\, \partial_x u & x \in \Omega_P, \\ u & x \in \Omega_H. \end{cases} \tag{1.4}$$

To specify boundary conditions, a minimal requirement for the solution to (1.3) to be extendable by 2-periodicity as a weak solution to (1.1) on the whole real line is the continuity of the flux $\mathscr{F}$ at any interface where the diffusion coefficient $\alpha(x)$ is discontinuous. This property holds in particular at $1^-/1^+$ (transition from parabolic to hyperbolic zone) and at $2^-/0^+$ (transition from hyperbolic to parabolic zone), yielding

$$\begin{cases} u(1^-,t) - \alpha_0 \partial_x u(1^-,t) = u(1^+,t), \\ u(0^+,t) - \alpha_0 \partial_x u(0^+,t) = u(2^-,t). \end{cases} \tag{1.5}$$

The continuity of the flux is physically important since it expresses mass conservation. In contrast, no continuity conditions are imposed a priori on the solution $u$ at the interfaces. The goal of this paper is twofold. First we present a mathematical setting in which (1.3)–(1.4)–(1.5) is well-posed. Second, we give reference solutions computed numerically for various sets of data $u_0$, $f$, and $\alpha_0$ in order to provide an interesting benchmark test suite.

Concerning the mathematical setting, it is important to observe that Problem (1.3)–(1.4)–(1.5) is ill-posed in the sense that it admits many solutions. To illustrate this point, consider the case of a null initial condition, $u_0 = 0$, and null source term, $f = 0$. Consider any smooth function of time $\varphi : \mathbb{R}^+ \to \mathbb{R}$ such that $\varphi^{(n)}(0) = 0$ for all $n \geqslant 0$ (for example $\varphi(t) = \alpha \exp(-\beta/t)$ with two constants $\alpha$ and $\beta > 0$). Impose the flux at $x = 1$ by setting $\mathscr{F}(t,1) = \varphi(t)$. One can easily show that the flux at $x = 2$ is a smooth function of time given by $\mathscr{F}(t,2) = \varphi(t-1)1_{t \geqslant 1}$. Moreover, there exists a smooth solution to the following parabolic problem on $(0,1)$ with Robin boundary conditions:

$$\begin{cases} \partial_t u + \partial_x u - \alpha_0\, \partial_{xx} u = 0 & (t,x) \in [0,\infty) \times (0,1), \\ \left(u - \alpha_0\, \partial_x u\right)(t,1) = \varphi(t), & t \in [0,\infty), \\ \left(u - \alpha_0\, \partial_x u\right)(t,0) = \varphi(t-1)1_{t \geqslant 1}, & t \in [0,\infty), \\ u(0,x) = 0, & x \in (0,1), \end{cases} \tag{1.6}$$

from which it is straightforward to build a nonzero smooth solution to (1.3)–(1.4)–(1.5) with data $u_0 = 0$ and $f = 0$. Thus, an additional condition has to be specified to recover uniqueness, i.e., to select the unique "physically acceptable" solution. This difficulty has been analyzed in [9] for one-dimensional coupled parabolic/hyperbolic problems using vanishing viscosity techniques. It results from this study that the physically acceptable solution is continuous at the interface where the flow leaves the parabolic zone to enter the hyperbolic one, whereas no continuity condition holds a priori at the other interface. In Section 2, we make clear that this additional condition is indeed needed to derive an existence and uniqueness result in the framework of the evolution linear semi-groups theory; see [2,12]. In particular, we prove that the evolution operator associated with (1.3) is maximal and monotone provided its domain is restricted to those functions that are continuous at the parabolic to hyperbolic interface. We also discuss the regularity of the solutions to (1.3)–(1.4)–(1.5) when the initial condition is too rough to be in the domain of the evolution operator.

Concerning the numerical results, we stress that a robust scheme should find "automatically" the physically acceptable solution, i.e., the continuity of the solution at the parabolic to hyperbolic interface should not be explicitly enforced by the scheme. To assess the schemes, reference solutions are computed for various data sets (initial condition, diffusion coefficient, and source term) using a problem-specific scheme described in Section 3. In each case, we present solution profiles at different times and various functionals of the solution allowing to characterize the properties of the schemes to be tested. Of particular interest are the total energy and the value of the jump at the interface $2^-/0^+$, both as a function of time. In Section 4, these reference results are used to assess on relatively coarse meshes the robustness and accuracy of various schemes: a simple upwind scheme, a box-scheme introduced in [7], and a locally discontinuous Galerkin method derived in [3]. All of them capture the physically correct solution.

## 2. MATHEMATICAL ANALYSIS

The goal of this section is twofold. First we clarify the importance of the continuity of the solution at the parabolic to hyperbolic interface in the framework of the evolution linear semi-groups theory. Second we discuss the regularity of the solutions to the evolution problem when the initial condition is too rough to be in the domain of the evolution operator.

### 2.1. Evolution linear semi-groups theory

Without loss of generality, we assume in this section that $\alpha_0 = 1$. To alleviate the notation, the flux given by (1.4) is denoted by $\mathscr{F}(u)$ instead of $\mathscr{F}(x,u,\partial_x u)$. For a function $v$ which is smooth in $\Omega_P \cup \Omega_H$, we introduce the jumps $[v(1)] = v(1^+) - v(1^-)$ and $[v(2)] = v(0^+) - v(2^-)$. For functions only depending on the space variable, distributional derivatives are denoted by a subscript $x$. For a region $R \subset \Omega$, the $L^2(R)$-

inner product is denoted by $(\cdot,\cdot)_R$. Let $\mathscr{P}(\Omega)$ be the space of 2-periodic functions in $\mathscr{C}^\infty(\overline{\Omega})$ and let $H^1_{per}(\Omega)$ be the closure of $\mathscr{P}(\Omega)$ for the $H^1$-norm. Let

$$V = \{\, v \in H^2(\Omega_P) \cap H^1(\Omega_H),\ [\mathscr{F}(v)(1)] = [\mathscr{F}(v)(2)] = [v(1)] = 0 \,\}, \tag{2.1}$$

and consider the operator $A : D(A) \equiv V \to L^2(\Omega)$ defined by

$$Av = (\mathscr{F}(v))_x. \tag{2.2}$$

**Theorem 2.1.** *The operator $A : V \to L^2(\Omega)$ is the infinitesimal generator of a continuous semigroup of contractions $T(t) : L^2(\Omega) \to L^2(\Omega)$, $0 \leqslant t < \infty$.*

**Proof.** We use the Lumer–Phillips criterion [12, p. 14], i.e., we establish that $A$ is monotone and maximal; see Lemmas 2.1 and 2.2 below. □

**Corollary 2.1.** For all $u_0 \in D(A)$ and $f \in C^1([0,\infty[;L^2(\Omega))$, the evolution problem

$$\begin{cases} \frac{\mathrm{d}u}{\mathrm{d}t} + Au = f \quad \forall t \in [0,\infty[, \\ u(0) = u_0, \end{cases} \tag{2.3}$$

admits a unique solution $u \in C^1([0,\infty);L^2(\Omega)) \cap C^0([0,\infty);D(A))$. This solution satisfies the a priori estimates

$$\|u(t)\|_\Omega \leqslant \|u_0\|_\Omega \quad \text{and} \quad \|\tfrac{\mathrm{d}u}{\mathrm{d}t}\|_\Omega \leqslant \|Au_0\|_\Omega, \quad \forall t \in [0,\infty[. \tag{2.4}$$

**Proof.** See, e.g., [12, p. 102]. □

**Lemma 2.1.** *The operator A is monotone:*

$$\forall v \in D(A), \quad (v,Av)_\Omega \geqslant 0. \tag{2.5}$$

**Proof.** Using integration by parts and the periodicity of the flux at points $x = 1$ and $x = 2$, we infer for all $v \in D(A)$ that

$$\begin{aligned} (v,Av)_\Omega &= \int_0^1 v\,(\mathscr{F}(v))_x\,\mathrm{d}x + \int_1^2 v\,(\mathscr{F}(v))_x\,\mathrm{d}x \\ &= -\int_0^2 v_x\,\mathscr{F}(v) - \mathscr{F}(v)(1)[v(1)] + \mathscr{F}(v)(2)[v(2)] \\ &= \int_0^1 (v_x)^2\,\mathrm{d}x + \tfrac{1}{2}[v^2(1)] - \tfrac{1}{2}[v^2(2)] - v(1^+)[v(1)] + v(2^-)[v(2)] \\ &= \int_0^1 (v_x)^2\,\mathrm{d}x + \tfrac{1}{2}[v(2)]^2 - \tfrac{1}{2}[v(1)]^2. \end{aligned}$$

Since $v \in D(A)$, $[v(1)] = 0$ implying that $(v,Av)_\Omega \geqslant 0$. □

**Lemma 2.2.** *The operator A is maximal:*

$$\forall g \in L^2(\Omega), \quad \exists u \in D(A) \quad \textit{s.t.} \quad u + Au = g. \tag{2.6}$$

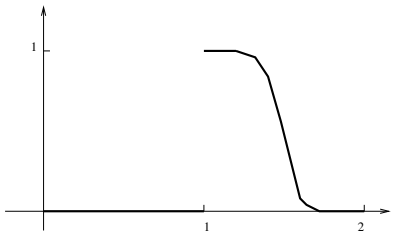


**Figure 1.** A suitable function $\psi$ for the proof of Lemma 2.2.

**Proof.** Let $g \in L^2(\Omega)$. The solution $u$ to (2.6) is constructed as the vanishing viscosity limit of a sequence of solution to a regularized problem. Henceforth, $c$ denotes a generic constant that may depend on $g$ but not on $\varepsilon$.
Step 1. Let $\varepsilon > 0$. For $v \in H^1_{per}(\Omega)$, define $\mathscr{F}^\varepsilon(v) = v - v_x$ in $(0,1)$, $\mathscr{F}^\varepsilon(v) = v - \varepsilon v_x$ in $(1,2)$, and $A^\varepsilon v = (\mathscr{F}^\varepsilon(v))_x$. Clearly, the problem

$$u^\varepsilon + A^\varepsilon u^\varepsilon = g, \tag{2.7}$$

admits a unique solution $u^\varepsilon \in H^1_{per}(\Omega)$. Multiplying (2.7) by $u^\varepsilon$ yields the following a priori estimates:

$$\|u^\varepsilon\|_{L^2(0,2)} \leqslant c, \tag{2.8}$$

$$\|u^\varepsilon\|_{H^1(0,1)} \leqslant c, \tag{2.9}$$

$$\sqrt{\varepsilon}\|u^\varepsilon\|_{H^1(1,2)} \leqslant c. \tag{2.10}$$

This implies $\|\mathscr{F}^\varepsilon(u^\varepsilon)\|_{L^2(0,2)} \leqslant c$. Moreover, $\|(\mathscr{F}^\varepsilon(u^\varepsilon))_x\|_{L^2(0,2)} \leqslant c$ since (2.7) holds in $L^2(\Omega)$, and multiplying (2.7) by a smooth 2-periodic function with support containing the point 2, we infer $[\mathscr{F}^\varepsilon(u^\varepsilon)(2)] = 0$. Therefore

$$\|\mathscr{F}^\varepsilon(u^\varepsilon)\|_{H^1_{per}(0,2)} \leqslant c. \tag{2.11}$$

The last important estimate consists in controlling the $H^1$-norm of $u^\varepsilon$ in the neighborhood of $x = 1$ uniformly in $\varepsilon$. Let $0 < \alpha < 1$. There exists a positive function $\psi$ which is zero on $(0,1)$ and on a neighborhood of 2, equal to one on the interval $[1, 1+\alpha]$, smooth over $(1,2)$, and non-increasing on the same interval; see Figure 1. Multiplying (2.7) by $u^\varepsilon_x \psi$ and integrating over $(1,2)$ yields

$$\int_1^2 u^\varepsilon u^\varepsilon_x \psi \,\mathrm{d}x + \int_1^2 (u^\varepsilon_x)^2 \psi \,\mathrm{d}x - \varepsilon \int_1^2 u^\varepsilon_{xx} u^\varepsilon_x \psi \,\mathrm{d}x = \int_1^2 f u^\varepsilon_x \psi \,\mathrm{d}x, \tag{2.12}$$

noticing that all the integrals are well-defined. Integrate by parts the third integral in the left-hand side to obtain

$$\int_1^2 u^\varepsilon_{xx} u^\varepsilon_x \psi \,\mathrm{d}x = -\frac{1}{2}\int_1^2 (u^\varepsilon_x)^2 \psi_x \,\mathrm{d}x + \frac{1}{2}(u^\varepsilon_x)^2(1), \tag{2.13}$$

whence we deduce

$$\int_1^2 (u_x^\varepsilon)^2\,\psi\,\mathrm{d}x \leqslant -\int_1^2 u^\varepsilon\,u_x^\varepsilon\,\psi\,\mathrm{d}x+\frac{\varepsilon}{2}\int_1^2 (u_x^\varepsilon)^2\,\psi_x\,\mathrm{d}x+\int_1^2 f\,u_x^\varepsilon\,\psi\,\mathrm{d}x. \tag{2.14}$$

Owing to the inequality $ab \leqslant \gamma a^2+\frac{1}{4\gamma}b^2$ valid for all $\gamma>0$, we infer

$$c\int_1^2 (u_x^\varepsilon)^2\,\psi\,\mathrm{d}x \leqslant \int_1^2 (u^\varepsilon)^2\,\psi\,\mathrm{d}x+\int_1^2 f^2\,\psi\,\mathrm{d}x+\frac{\varepsilon}{2}\int_1^2 (u_x^\varepsilon)^2\,|\psi_x|\,\mathrm{d}x, \tag{2.15}$$

whence we deduce using the above a priori estimates that

$$\|u^\varepsilon\|_{H^1(1-\alpha,1+\alpha)} \leqslant c. \tag{2.16}$$

Step 2. Using estimates (2.8), (2.9), and (2.11), one can extract a subsequence $u^{\varepsilon_n}$ such that

$$u^{\varepsilon_n} \rightharpoonup u \qquad \text{in } L^2(0,2), \tag{2.17}$$

$$u^{\varepsilon_n} \rightharpoonup u \qquad \text{in } H^1(0,1), \tag{2.18}$$

$$\mathscr{F}^{\varepsilon_n}(u^{\varepsilon_n}) \rightharpoonup \overline{\mathscr{F}} \qquad \text{in } H^1_{per}(0,2). \tag{2.19}$$

Passing to the limit in (2.7), we deduce that $u$ satisfies $u+Au=g$ in $\mathscr{D}'(0,1)$ and $\mathscr{D}'(1,2)$. Moreover, it is clear that $\overline{\mathscr{F}}=u-u_x$ in $(0,1)$. On the interval $(1,2)$, one has $u^{\varepsilon_n}-\mathscr{F}^{\varepsilon_n}(u^{\varepsilon_n})=\varepsilon_n u_x^{\varepsilon_n}$. The left-hand side converges to $u-\overline{\mathscr{F}}$ in $\mathscr{D}'(1,2)$ and the right-hand side converges to 0 in $L^2(0,1)$ owing to (2.10). Therefore, $\overline{\mathscr{F}}=u$ in $(1,2)$. We have thus shown that $\overline{\mathscr{F}}=\mathscr{F}(u)$ in $\Omega$, where $\mathscr{F}(u)$ is defined by (1.4). Since $\overline{\mathscr{F}}$ is in $H^1_{per}(0,2)$, we obtain $[\mathscr{F}(v)(1)]=[\mathscr{F}(v)(2)]=0$. Finally, using the estimate (2.16), we deduce that (up to the extraction of a new subsequence) the limit $u$ is continuous in a neighborhood of 1. In summary, $u\in D(A)$ and $u+Au=g$ in $L^2(\Omega)$, which concludes the proof. □

**Remark 2.1.** Clearly, the solution $u$ to (2.6) is unique since $u+Au=0$ and $u\in D(A)$ implies $\|u\|^2_{L^2(\Omega)}=0$ owing to the monotonicity of $A$. Therefore, the operator $(I+A)$ is bijective from $D(A)$ into $L^2(\Omega)$. Let $B:D(B)\equiv W\to L^2(\Omega)$ be the extension of $A$ to the space $W$ defined as in (2.1) by omitting the interface condition $[v(1)]=0$. Then, one readily verifies that the equation $u+Bu=0$ admits infinitely many solutions in $D(B)$, i.e., the operator $(I+B)$ is not injective from $D(B)$ to $L^2(\Omega)$.

**Remark 2.2.** Since $A$ is monotone and maximal and since $L^2(\Omega)$ is reflexive, its domain $D(A)$ is dense in $L^2(\Omega)$; see, e.g., [12, p. 16]. Moreover, for all $\lambda>0$, the operator $(I+\lambda A)$ is bijective from $D(A)$ to $L^2(\Omega)$, $(I+\lambda A)^{-1}$ is bounded in $L^2(\Omega)$, and $\|(I+\lambda A)^{-1}\|_{\mathscr{L}(L^2(\Omega))}\leqslant 1$; see, e.g., [1].

**Remark 2.3.** The argument in the proof of Lemma 2.2 cannot be used to prove that the $H^1$-norm of $u^\varepsilon$ is uniformly bounded on a left neighborhood of 2 with the function $\varphi(x) = \psi(3-x)$. Indeed, after integration by parts, one obtains

$$-\int_1^2 u^\varepsilon_{xx}\, u^\varepsilon\, \varphi \,\mathrm{d}x = \frac{1}{2}\int_1^2 (u^\varepsilon_x)^2\, \varphi_x \,\mathrm{d}x - \frac{1}{2}(u^\varepsilon_x)^2(2), \tag{2.20}$$

and one cannot conclude because of the sign of the last term in the right-hand side.

## 2.2. Rough initial data

In this section we construct a weak solution to the evolution problem (1.3)–(1.4) when the initial condition $u_0$ is too rough to be in the domain of $A$, e.g., $u_0 \in L^2(\Omega)$ only. We limit ourselves to the homogeneous case, $f \equiv 0$. Our main result is that under some assumptions, once the initial condition has crossed the whole hyperbolic zone, i.e., at time $t > 1$, the solution we construct is smooth enough to be in $D(A)$.

Let $Y = L^\infty((0,\infty);L^2(\Omega_P)) \cap L^2((0,\infty);H^1(\Omega_P)) \cap L^2((0,\infty);L^2(\Omega_H))$. To construct a weak solution to (1.3)–(1.4) in $Y$, one proceeds as follows. First solve the mixed Robin–Neumann problem: Seek $u \in L^\infty((0,\infty);L^2(\Omega_P)) \cap L^2((0,\infty);H^1(\Omega_P))$ such that $u_P(t=0,\cdot) = u_{0|\Omega_P}$ and, $\forall \varphi \in H^1(\Omega_P)$ and a.e. in $t$,

$$(\partial_t u_P, \varphi)_{\Omega_P} - (u_P - \partial_x u_P, \partial_x \varphi)_{\Omega_P} + u_P(t,1)\varphi(1) = \psi(t)\varphi(0), \tag{2.21}$$

where

$$\psi(t) = \begin{cases} u_0(2-t) & \text{if } t < 1, \\ u_P(t-1,1) & \text{if } t > 1. \end{cases} \tag{2.22}$$

One readily checks that Problem (2.21) is well-posed. The unique solution $u_P$ solves the evolution equation (1.3)–(1.4) in $\mathscr{D}'((0,\infty)\times\Omega_P)$ and satisfies weakly the Robin condition $\mathscr{F}(u)(t,0) = \psi(t)$ and the Neumann condition $\partial_x u_P(t,1) = 0$. Second, use the value $u_P(1,t)$ to feed the advection equation

$$\partial_t u_H + \partial_x u_H = 0, \quad \text{in } \mathscr{D}'((0,\infty)\times\Omega_H). \tag{2.23}$$

Then, set $u_{|\Omega_P} = u_P$ and $u_{|\Omega_H} = u_H$. It is clear that $u \in Y$, $u$ is a weak solution to (1.3)–(1.4) in $\mathscr{D}'((0,\infty)\times\Omega)$, $u$ is continuous at $x = 1$, and the flux $\mathscr{F}(u)$ satisfies weakly the interface conditions. The condition at the interface $2^-/0^+$ results from the Robin condition and the fact that $u_H(t,2) = u_P(t-1,1)$ whereas the condition at the interface $1^-/1^+$ results from the homogeneous Neumann condition and the fact that the solution $u$ is continuous at $x = 1$. Furthermore, it is clear that there is a unique $u \in Y$ satisfying the above properties.

To obtain stronger regularity results on the solution $u \in Y$ constructed above, we slightly restrict the class of initial conditions. The proofs below are only sketched since they use well-known techniques based on energy estimates; see, e.g., [11,13].

**Lemma 2.3.** *Let $u_0 \in H^1(\Omega) \cap H^2(\Omega_P)$. Then, the solution $u \in Y$ constructed above is in $C^1((0,\infty);L^2(\Omega)) \cap C^0((0,\infty);D(A))$.*

**Proof.** Since $u_0 \in H^1(\Omega_H)$, we infer $\psi \in H^1(0,1)$ in time. Testing the time-derivative of (2.21) by $\partial_t u_P$ (this can be justified rigorously by first working in finite dimension and then passing to the limit; see, e.g., [11, p. 80]) yields

$$\frac{1}{2}\frac{\mathrm{d}}{\mathrm{d}t}\|\partial_t u_P\|^2_{\Omega_P} + \|\partial_{xt} u_P\|^2_{\Omega_P} - (\partial_t u_P, \partial_{xt} u_P)_{\Omega_P} + (\partial_t u_P(t,1))^2 = \psi'(t)\partial_t u_P(t,0). \tag{2.24}$$

Using Young's inequality to hide the third term in the left-hand side and the right-hand side, dropping the fourth term, and then using a Gronwall's Lemma, we infer, for all $0 < T < 1$,

$$\|\partial_t u_P(T,\cdot)\|^2_{\Omega_P} + \int_0^T \|\partial_{xt} u_P\|^2_{\Omega_P}\,\mathrm{d}t \leqslant c(\|\psi\|^2_{H^1(0,1)} + \|\partial_t u_P(0,\cdot)\|^2_{\Omega_P}). \tag{2.25}$$

To prove that the last term in the right-hand side is controlled, one works in finite dimension and uses the fact that $u_0 \in H^1(\Omega) \cap H^2(\Omega_P)$. To sum up, we obtain $\partial_t u_P \in L^\infty((0,\infty);L^2(\Omega_P)) \cap L^2((0,\infty);H^1(\Omega_P))$. As a result, $t \mapsto u_P(t,x=1)$ is in $H^1$ in time; hence, $u_H(t,\cdot)$ is smooth for $t > 0$, and therefore, $u(t,\cdot)$ is in $D(A)$ for $t > 0$. We conclude using the uniqueness of the solution given by the evolution semi-groups theory. □

**Proposition 2.1.** *Let $u_0 \in L^2(\Omega_P) \cap L^2(\Omega_H)$. Then, the solution $u \in Y$ constructed above is in $C^1((1,\infty);L^2(\Omega)) \cap C^0((1,\infty);D(A))$. Moreover, for $0 < t \leqslant 1$, $u$ is a strong solution to* (1.3)–(1.4) *except on the line $x = 1+t$, and the matching conditions on the flux and on the solution hold strongly for $t \in (0,1)$.*

**Proof.** First observe that for an arbitrarily small time $\varepsilon$, $u_P(\varepsilon,\cdot)$ is in $H^1(\Omega_P)$. Testing (2.21) by $\partial_t u_P$ (this can be justified rigorously; see, e.g., [13, p. 370]) and proceeding as in the previous proof, one can prove that, for $\varepsilon < T < 1$,

$$\|u_P(T,\cdot)\|^2_{H^1(\Omega_P)} + \int_\varepsilon^T \|\partial_t u_P(t,\cdot)\|^2_{\Omega_P}\,\mathrm{d}t \leqslant c(\|u_P(\varepsilon,\cdot)\|^2_{H^1(\Omega_P)} + \int_\varepsilon^T \psi(t)^2\,\mathrm{d}t), \tag{2.26}$$

whence we deduce $u_P \in L^\infty((\varepsilon,1);H^1(\Omega_P)) \cap H^1((\varepsilon,1);L^2(\Omega_P))$. It is then straightforward to show that for an arbitrarily small time $\varepsilon$, $u(\varepsilon,\cdot) \in H^1(\Omega) \cap H^2(\Omega_P)$. Using $u(\varepsilon,\cdot)$ as an initial condition and reasoning as in the proof of Lemma 2.3, we infer that $\partial_t u_P \in L^\infty((\varepsilon,1);L^2(\Omega_P)) \cap L^2((\varepsilon,1);H^1(\Omega_P))$. It is then clear that $u(1,\cdot)$ is in $H^1(\Omega) \cap H^2(\Omega_P)$, showing that $u \in C^1((1,\infty);L^2(\Omega)) \cap C^0((1,\infty);D(A))$. The case $t \in (0,1)$ is straightforward. □

**Remark 2.4.** Assume that $u_0$ is continuous at $x = 1$ and is piecewise $H^1$ in $\Omega_H$, i.e., there exists a finite sequence $1 < t_1 < \cdots < t_N < 2$ such that $u_{-\Omega_H} \in H^1(1,t_1) \cup \cdots \cup H^1(t_N,1)$. Then, the solution $u \in Y$ constructed above is in $C^1((t_*,\infty);L^2(\Omega)) \cap$

$C^0((t_*,\infty);D(A))$ where $t_* = 2-t_1$ is the time for which the last singularity in $u_0$ has crossed $\Omega_H$. See test cases 2 and 3 in Section 3.2.

**Remark 2.5.** Let $u^\varepsilon$ be the time-dependent solution of the evolution problem in which a small diffusion coefficient $\varepsilon$ is added in $\Omega_H$. Then, if $u_0 \in H^2(\Omega)$, one can show that $u^\varepsilon$ converges to $u \in Y$, the weak solution constructed above, at least in the distribution sense. This justifies the fact that the continuity condition for the solution at $x = 1$ can be captured by a vanishing viscosity technique.

## 3. REFERENCE SOLUTIONS

This section presents reference solutions for the evolution problem (1.3)–(1.4)–(1.5) for various sets of data. Reference solutions are obtained computationally using a problem-specific scheme with built-in interface condition.

### 3.1. A scheme with built-in interface condition

The idea is to use continuous piecewise-linear finite elements to discretize the advection-diffusion equation in $\Omega_P$ and to use exact integration along characteristics to solve the purely advective equation in $\Omega_H$. To simplify the presentation, we assume that the source term $f$ is identically zero on $\Omega_H$. The scheme can be easily extended to the general case by appropriate integration in time along the characteristics.

Let $u$ solve (1.3)–(1.4)–(1.5) and let $\varphi_1(t) = \mathscr{F}(u)(t,1)$ be the yet unknown flux at point $x = 1$. Since $u(t,1^+) = \varphi_1(t)$, the purely advective equation can be integrated exactly on $\Omega_H$ to yield the flux at point $x = 2$:

$$\varphi_2(t) = u(t,2^-) = \begin{cases} u_0(2-t) & \text{if } t \leqslant 1, \\ \varphi_1(t-1) & \text{if } t \geqslant 1. \end{cases} \tag{3.1}$$

Using the periodicity of the flux, we infer that the restriction of the solution $u$ to the parabolic subdomain $\Omega_P$ satisfies the following evolution problem with Robin boundary conditions:

$$\begin{cases} \partial_t u + \partial_x u - \alpha_0 \partial_{xx} u = f & (t,x) \in [0,\infty) \times (0,1), \\ \left(u - \alpha_0 \partial_x u\right)(t,1) = \varphi_1(t) & t \in [0,\infty), \\ \left(u - \alpha_0 \partial_x u\right)(t,0) = \varphi_2(t) & t \in [0,\infty), \\ u(0,x) = 0 & x \in (0,1). \end{cases} \tag{3.2}$$

Let $\mathscr{M}_P = \cup_{j=1}^{N_P} [x_j, x_{j+1}]$ be a mesh of $\Omega_P$. Denote by $V_P$ the space spanned by continuous piecewise-linear functions on this mesh. The finite element approximation to (3.2) consists of seeking $u_h \in C^1([0,\infty[;V_P)$ such that $\forall v_h \in V_P$ and $t \geqslant 0$,

$$\tfrac{\mathrm{d}}{\mathrm{d}t}(u_h, v_h)_{\Omega_P} - (\mathscr{F}(u_h), v_{h,x})_{\Omega_P} + \varphi_1(t)\, v_h(1) - \varphi_2(t)\, v_h(0) = (f, v_h)_{\Omega_P}. \tag{3.3}$$

Equation (3.3) is discretized in time by an implicit Euler scheme, yielding

$$\tfrac{1}{\delta t}(u_h^{n+1}-u_h^n,v_h)_{\Omega_P}-(\mathscr{F}(u_h^{n+1}),v_{h,x})_{\Omega_P}+\varphi_1(t^{n+1})\,v_h(1)-\varphi_2(t^{n+1})\,v_h(0)=(f,v_h)_{\Omega_P}, \tag{3.4}$$

where $\delta t \leqslant 1$ is the time step. Owing to (3.1), the flux $\varphi_2(t^{n+1})$ can be evaluated explicitly using known values of the initial condition and of the flux $\varphi_1(t)$ at previous time steps. The unknown flux $\varphi := \varphi_1(t^{n+1})$ is determined by the interface condition $[u(1)] = 0$ at time $t^{n+1}$. Since this jump is an affine function of $\varphi$, it is straightforward to determine the correct value for $\varphi$ by evaluating the jump with two arbitrary trial values for $\varphi$ and using linear interpolation. To sum up, our time-marching algorithm proceeds as follows:

1. Select two trial values for $\varphi$ and evaluate for each of these values the approximate solution $u_h^{n+1}$ by solving the linear system (3.4).
2. Determine using linear interpolation the correct value of the flux (ensuring the zero-jump condition) and the corresponding solution $u_h^{n+1}$.

### 3.2. Test cases

To illustrate the above algorithm and the physical behavior of the solutions to the evolution problem (1.3)–(1.4), we consider the following test cases:

- Case 1 (smooth initial data, small diffusion coefficient): $\alpha_0 = 0.05$, $f = 0$, and $u_0(x) = 16x^2(1-x)^2 1_{[0;1]}(x)$.
- Case 2 (rough initial data, small diffusion coefficient): $\alpha_0 = 0.05$, $f = 0$, and $u_0(x) = 1_{[1.;1.25]}(x)$.
- Case 3 (rough initial data, large diffusion coefficient): $\alpha_0 = 1$, $f = 0$, and $u_0(x) = 1_{[1.;1.25]}(x)$.

Numerical simulations are performed on the time interval $(0,5)$ using $10^6$ time steps and a uniform mesh of $(0,1)$ with cell spacing $h = 10^{-3}$. Figures 2–4 present the following results:

- The energy $\mathscr{E}(t)$ defined as

$$\mathscr{E}(t) = \frac{1}{2}\int_0^2 u(t,x)^2\,\mathrm{d}x + \alpha_0\int_0^t\left(\int_0^1(\partial_x u(t,x))^2\,\mathrm{d}x\right)\mathrm{d}t, \tag{3.5}$$

  and normalized by $\mathscr{E}(0)$, and the $L^\infty(\Omega)$-norm of $u$, both quantities as a function of time. We infer from Lemma 2.1 that

$$\forall t \geqslant 0, \quad \frac{\mathrm{d}}{\mathrm{d}t}\mathscr{E}(t) \leqslant 0. \tag{3.6}$$

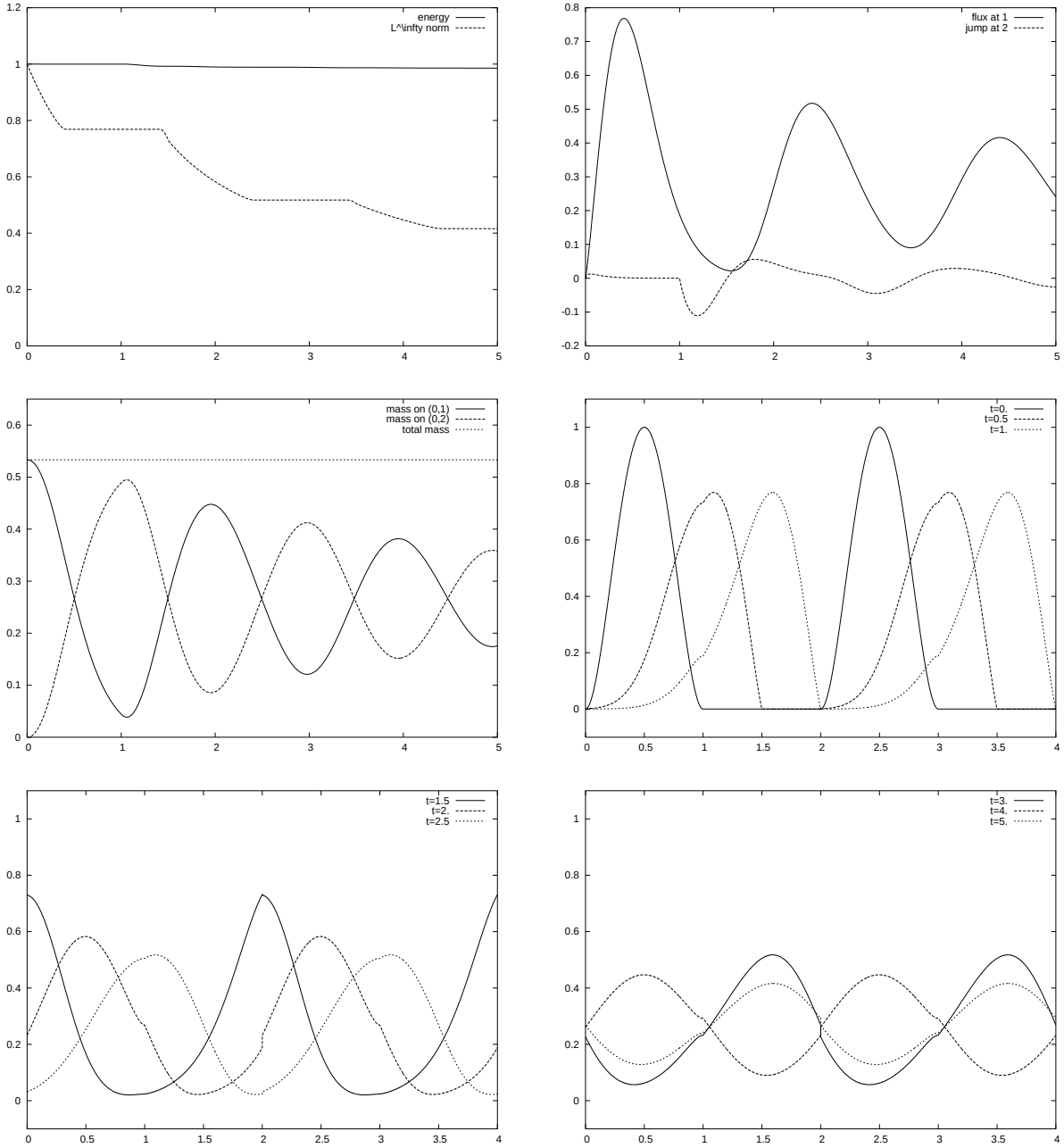


**Figure 2.** Reference solution for case 1 ($\alpha = 0.05$, $f = 0$, and $u_0(x) = 16x^2(1-x)^2 1_{[0;1]}(x)$).

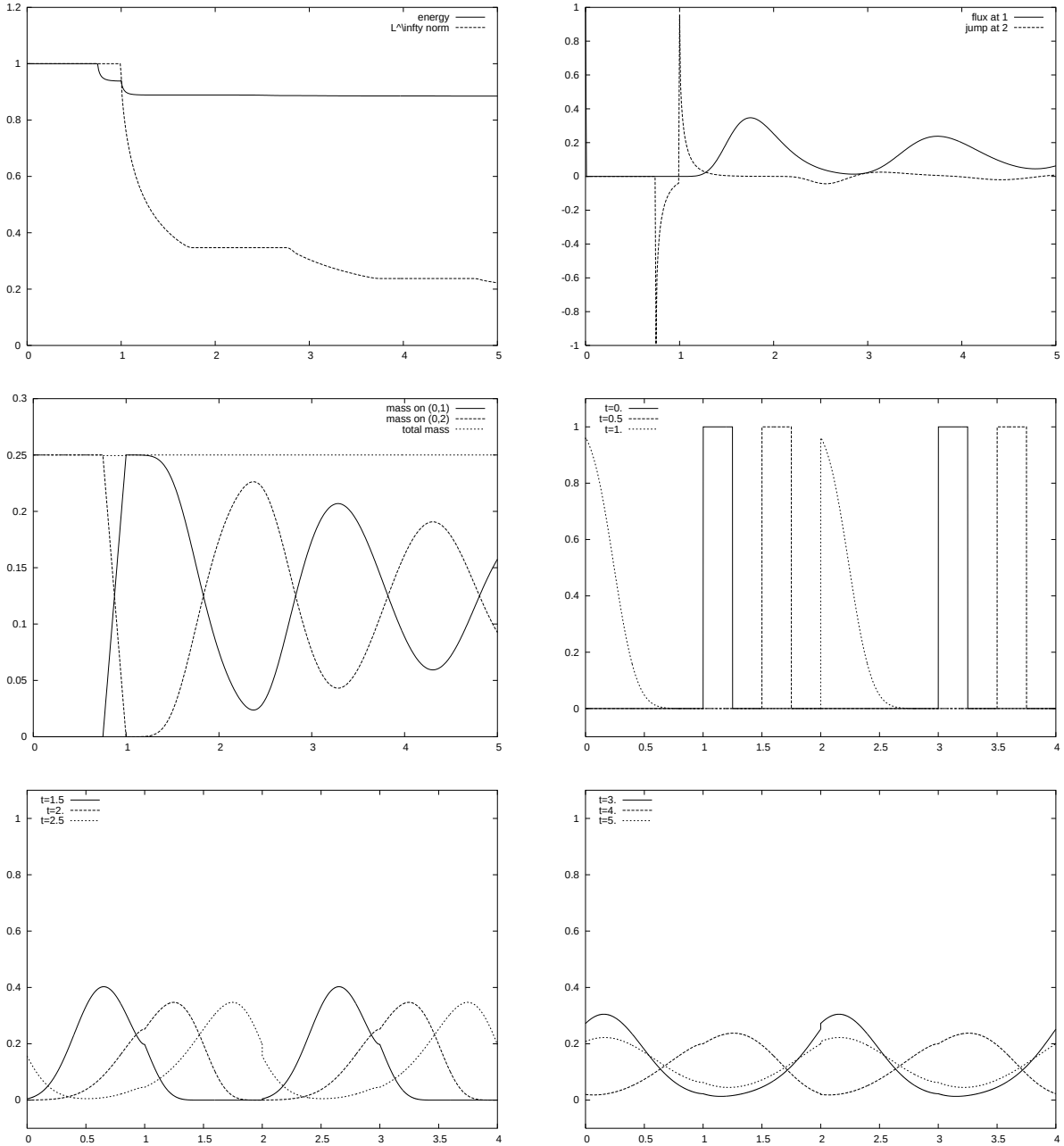


**Figure 3.** Reference solution for case 2 ($\alpha = 0.05$, $f = 0$, and $u_0(x) = 1_{[1.;1.25]}(x)$).

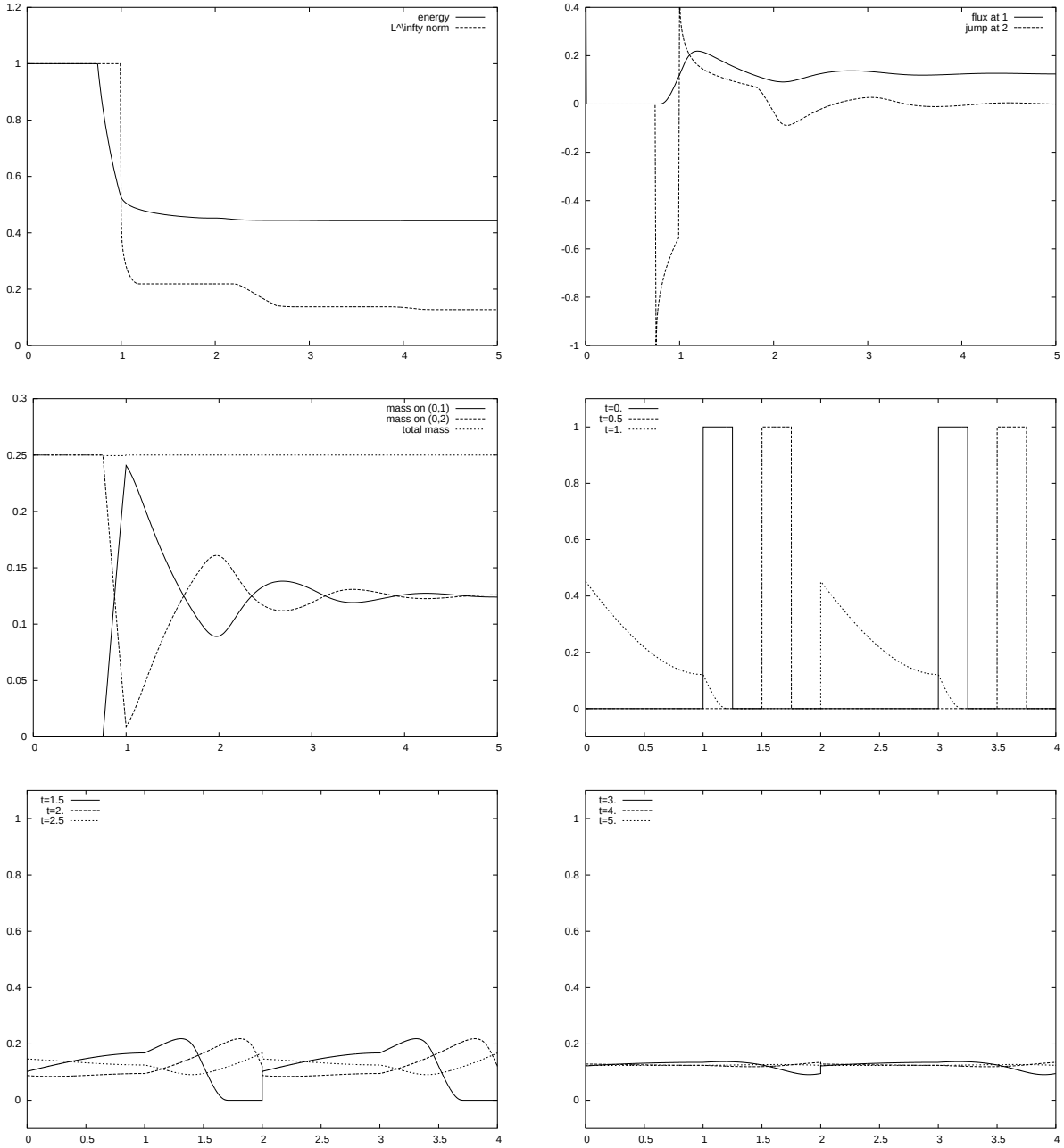


**Figure 4.** Reference solution for case 3 ($\alpha = 1.$, $f = 0$, and $u_0(x) = 1_{[1.;1.25]}(x)$).

- The flux at $x = 1$ and the jump at $x = 2$, as a function of time.
- The masses $\int_0^1 u$, $\int_1^2 u$, and $\int_0^2 u$ as a function of time. Note that owing to the periodicity of the flux, the following mass conservation property holds:

$$\forall t \geqslant 0, \quad \frac{\mathrm{d}}{\mathrm{d}t} \int_0^2 u(t,x)\,\mathrm{d}x = \int_0^2 f(t,x)\,\mathrm{d}x. \tag{3.7}$$

- The profiles $x \mapsto u(t,x)$ (represented on $(0,4)$ to illustrate periodicity) at times $t = 0$, 0.5, 1, 1.5, 2, 2.5, 3, 4, and 5.

For case 1 where the initial data is smooth (see Figure 2), a very small amount of energy is dissipated. The jump at point $x = 2$ is initially zero, but takes nonzero values with peaks in the time interval $1 \leqslant t \leqslant 2$ after the initial data has reached the hyperbolic to parabolic interface. The discontinuity is clearly visible in the bottom left panel of Figure 2. We also observe the homogeneous Neumann condition $\partial_x u_h(t,1^-) = 0$ for all $t > 0$, which is a direct consequence of the flux continuity at point $x = 1$ together with the zero-jump condition $[u_h(1)] = 0$.

For case 2 (see Figure 3), the singularities in the initial data appear clearly in the jump at $x = 2$. The two peaks in the upper right panel of Figure 3 correspond to the times when the leading and trailing edge of the wave reach the point $x = 2$. Once the initial data has crossed into the parabolic subdomain, it is dissipated and the jump takes much smaller values. The homogeneous Neumann condition at point $x = 1$ is again clearly visible in the solution profiles. Similar conclusions can be drawn for case 3 (see Figure 4). An important difference for case 3 is the larger amount of energy dissipation owing to the larger value of the diffusion coefficient. As a result, the second singularity in the jump is much smaller than for case 2 (0.4 instead of 1).

Convergence tests are presented in Table 1 for case 1. The solution presented in Figure 2, say $u_{\mathrm{ref}}$, is used as a reference to evaluate the errors associated with approximate solutions obtained on coarser grids and with larger time steps. Let $u_{h\delta t}$ be the approximate solution and $e = u_{\mathrm{ref}} - u_{h\delta t}$ be the error. We consider the following measures of the error:

- $\|e(t,\cdot)\|_{L^\infty(\Omega)}$ at times $t = 1$ and $t = 5$.
- $\|\mathscr{F}\|_{\ell^p(0,5)}$, the error in the flux at point $x = 1$ for $0 \leqslant t \leqslant 5$, for $p = 1$ and $p = \infty$.
- $\|\mathscr{E}\|_{\ell^p(0,5)}$, the error in the energy for $0 \leqslant t \leqslant 5$, for $p = 1$ and $p = \infty$.

Recall that for a discrete sequence in time $v(n\delta t)_{0 \leqslant n\delta t \leqslant T} \in \mathbb{R}^M$ with $M = \sum_{0 \leqslant n\delta t \leqslant T} 1$, one can consider the discrete norms $\|v\|_{\ell^1(0,T)} = \frac{1}{M} \sum_{0 \leqslant n\delta t \leqslant T} |v(n\delta t)|$ and $\|v\|_{\ell^\infty(0,T)} = \max_{0 \leqslant n\delta t \leqslant T} |v(n\delta t)|$. The results presented in Table 1 show that the scheme is second-order in space and first-order in time for the three error measures, in agreement with theoretical predictions.

| | | $\|e(t,\cdot)\|_{L^\infty(\Omega)}$ | | $\|\mathscr{F}\|_{\ell^p(0,5)}$ | | $\|\mathscr{E}\|_{\ell^p(0,5)}$ | |
|---|---|---|---|---|---|---|---|
| $h$ | $\delta t$ | $t=1$ | $t=5$ | $p=\infty$ | $p=1$ | $p=\infty$ | $p=1$ |
| 0.02 | $10^{-6}$ | 1.1e-3 | 7.4e-4 | 1.1e-3 | 4.1e-4 | 1.6e-4 | 4.3e-5 |
| 0.01 | $10^{-6}$ | 2.6e-4 | 1.8e-4 | 2.6e-4 | 1.0e-4 | 4.0e-5 | 1.1e-5 |
| 0.005 | $10^{-6}$ | 6.4e-5 | 4.5e-5 | 6.4e-5 | 2.5e-5 | 1.0e-5 | 2.6e-6 |
| 0.02 | $2\times10^{-5}$ | 2.0e-4 | 1.8e-4 | 2.2e-4 | 9.8e-5 | 1.3e-4 | 9.3e-5 |
| 0.02 | $10^{-5}$ | 9.3e-5 | 8.7e-5 | 1.0e-4 | 4.7e-5 | 6.0e-5 | 4.4e-5 |
| 0.02 | $5\times10^{-6}$ | 4.2e-5 | 3.9e-5 | 4.5e-5 | 2.1e-5 | 3.0e-5 | 2.0e-5 |

**Table 1.** Convergence analysis: $h$ denotes the space step and $\delta t$ the time step. The errors in the first three lines are scaled by $10^2$ and those in the last three lines by $10^3$.

## 4. RESULTS WITH GLOBAL SCHEMES

This section presents results obtained with schemes in which the continuity of the solution at the parabolic to hyperbolic interface is not enforced explicitly. We consider a simple upwind scheme, a finite volume box-scheme introduced in [7], and a local discontinuous Galerkin method derived in [3]. These schemes are able to select automatically the physically acceptable solution.

### 4.1. Upwind scheme

To illustrate the numerical results that can be obtained for the evolution problem (1.3)–(1.4) with a very simple scheme, we consider in this section a continuous piecewise-linear finite element method on $(0,2)$ with periodic conditions on the solution and with first-order artificial viscosity in the hyperbolic subdomain $\Omega_H$. The mesh is uniform with step size $h$, and the artificial viscosity is set to $\varepsilon = \frac{h}{2}$. The numerical scheme is equivalent to discretizing the spatial derivatives with centered differences in $\Omega_P$ and an upwind scheme in $\Omega_H$. In both subdomains, time integration is performed using an implicit Euler scheme without lumping of the mass matrix. The time step is set to $\delta t = 10^{-4}$. Two meshes of $\Omega$ are considered, one with 200 cells and one with 400 cells. The corresponding numerical solutions are termed the "coarse grid/upwind" solution and the "fine grid/upwind solution."

Numerical results are presented in Figure 5. For the sake of brevity, we only show the time evolution of the normalized energy, the $L^\infty(\Omega)$-norm of the solution, the flux at $x=1$, and the jump at $x=2$ estimated by the difference $u(t,2)-u(t,2-h)$. To facilitate comparisons with the reference solutions, these quantities are plotted using the same scale as in the two upper panels of Figures 2–4. In all cases, the correct physical behavior is captured, confirming that the vanishing viscosity solution can capture the physically relevant interface condition on the solution. For case 1 where the initial data is smooth, the coarse grid/upwind solution, the fine grid/upwind solution, and the reference solution agree well. Minor discrepancies between coarse and fine grid solutions are observed in the energy profile. The situation is different for case 2 where the initial data is rough. Owing to the high level of

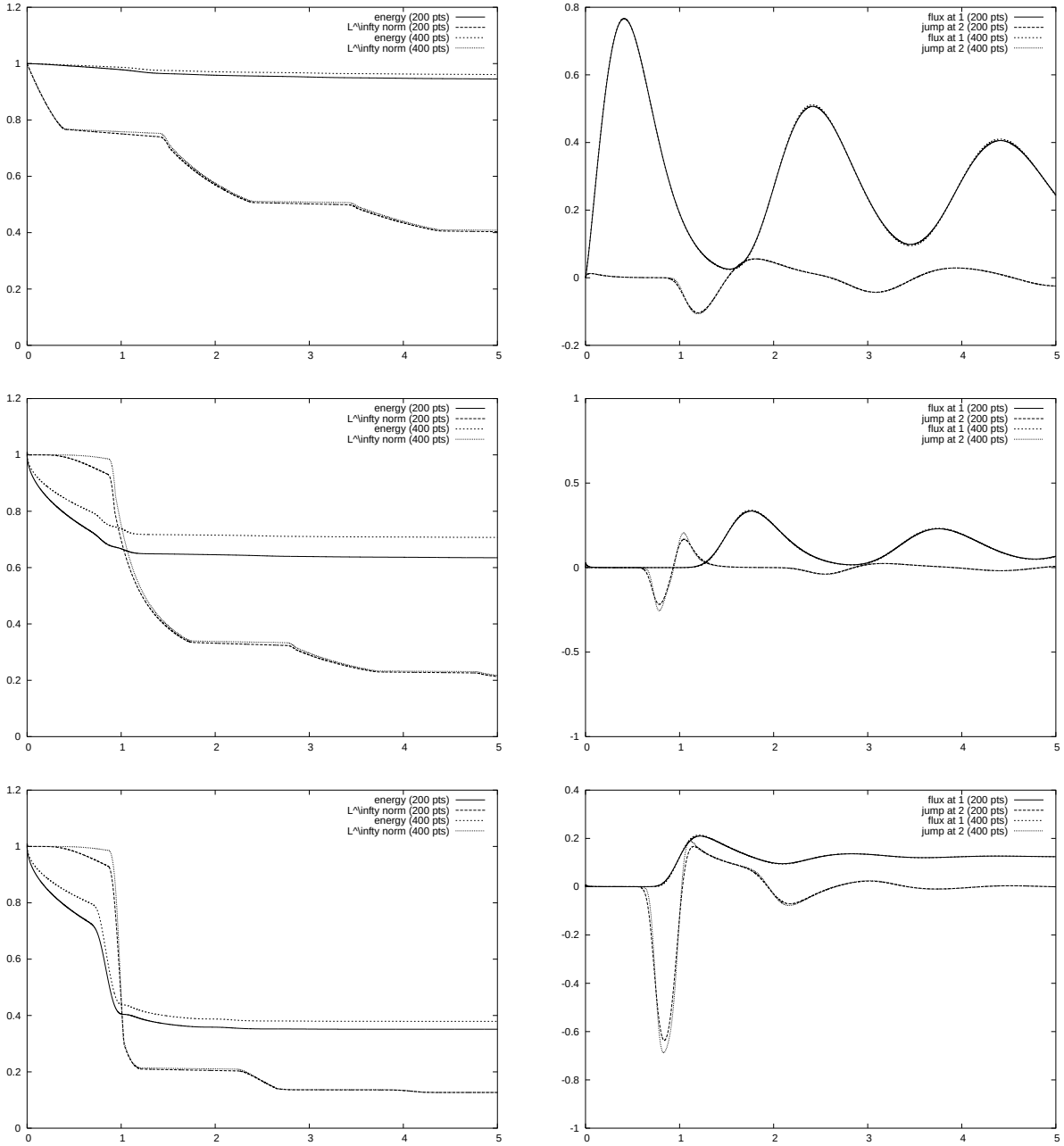


**Figure 5.** Numerical results obtained with the upwind method: case 1 (top), case 2 (center), and case 3 (bottom). Left panels: normalized energy and $L^\infty(\Omega)$-norm of the solution; right panels: the flux at $x = 1$ and the jump at $x = 2$.

dissipation induced by the scheme, significant errors are observed in the energy and jump profiles even on the fine grid/upwind solution. The singularities in the jump as the leading and trailing edges of the initial condition leave the hyperbolic subdomain to enter the parabolic subdomain are clearly under-resolved. Moreover, the asymptotic value of the energy (at time $t = 5$) is underestimated by 28.1% with the coarse grid/upwind solution and by 19.9% with the fine grid/upwind solution. The same conclusions hold for case 3 although the diffusion coefficient is larger.

### 4.2. A highly accurate box-scheme

The box-scheme that we use to simulate the evolution problem is a high order box-scheme introduced in [7]. Box-schemes, like the Preissmann scheme, are commonly used in surface flow simulations (e.g., river flows, dam breaking) as well as in groundwater flow simulations (e.g., sedimentation, pollutant transport); see [10].

We shortly present the main features of our box-scheme. First, equation (1.3) is recast in mixed form using the diffusive flux $p(x) = -\alpha(x)u_x$ as an auxiliary unknown. This yields

$$\begin{cases} \partial_t u + \partial_x(u+p) = f & (t,x) \in [0,\infty) \times (0,2), \\ p = -\alpha(x)\,\partial_x u & (t,x) \in [0,\infty) \times (0,2), \\ (u+p)(t,0) = (u+p)(t,2), & t \in [0,\infty), \\ u(0,x) = u_0,\ p(0,x) = -\alpha(x)\,u_0'(x) & x \in (0,2). \end{cases} \tag{4.1}$$

The viscosity is $\alpha(x) = \alpha_0$ if $x \in (0,1)$ and $\alpha(x) = 0$ if $x \in (1,2)$. Let $\mathscr{M} = \cup_{j=1}^{N}[x_j, x_{j+1}]$ be a mesh of $\Omega$, $\delta t$ be the time step, and set $t^n = n\delta t$. Set $h_{j-1/2} = x_j - x_{j-1}$ and introduce the box $K_{j-1/2} = [x_{j-1}, x_j]$ for $2 \leqslant j \leqslant N+1$. We assume that $\alpha$ is constant on each box, and we set $\alpha_{j-1/2} = \alpha_{|K_{j-1/2}}$. Taking the mean value of the first two equations in (4.1) on a box $K_{j-1/2}$ yields the following identities verified by the *exact solution*:

$$h_{j-1/2}\,\frac{\mathrm{d}}{\mathrm{d}t}(\overline{\Pi^0 u})_{|j-1/2}(t) + [\mathscr{F}(x_j,t) - \mathscr{F}(x_{j-1},t)] = h_{j-1/2}\,(\Pi^0 f)_{|j-1/2}(t), \tag{4.2}$$

$$h_{j-1/2}\,(\Pi^0 p)_{|j-1/2}(t) = -\alpha_{j-1/2}\,[u(x_j,t) - u(x_{j-1},t)], \tag{4.3}$$

where $\Pi^0$ denotes the averaging operator on the boxes and $\mathscr{F}(x_j,t) = u(x_j,t) + p(x_j,t)$. The box scheme evolves simultaneously 3 quantities:

- The values $u_j^n$ and $p_j^n$ at the points of the mesh; these values are such that $u_j^n \simeq u(x_j,t^n)$ and $p_j^n \simeq p(x_j,t^n) = -\alpha(x_j)u_x(x_j,t^n)$.

- The value $\bar{u}_{j-1/2}$ in each box $K_{j-1/2}$ defined as $\bar{u}_{j-1/2}^n \simeq \frac{1}{h_{j-1/2}}\int_{x_{j-1}}^{x_j} u(x,t^n)\,\mathrm{d}x$.

Using a $\vartheta$-scheme for the time integration of (4.2) yields

$$\delta\overline{u}^n_{j-1/2} = -\frac{1}{h_{j-1/2}}(F^n_j - F^n_{j-1}) - \frac{\vartheta\,\delta t}{h_{j-1/2}}\,(\delta u^n_j + \delta p^n_j - \delta u^n_{j-1} - \delta p^n_{j-1}) + \mathscr{R}^n_{j-1/2}(f), \tag{4.4}$$

where $F^n_j = u^n_j + p^n_j$ and $\mathscr{R}^n_{j-1/2}(f) = (1-\vartheta)(\Pi^0 f)_{|j-1/2}(t^n) + \vartheta\,(\Pi^0 f)_{|j-1/2}(t^{n+1})$. In addition, we have introduced the discrete time derivative operator $\delta$ such that for a time discrete sequence $(Z^n)_{n\geqslant 0}$, we have $\delta Z^n = \frac{Z^{n+1}-Z^n}{\delta t}$. The relation (4.4) only contains the parameter $\vartheta$ selected for the time scheme.

The second relation used in the box-scheme expresses the link between the incremental value of $\delta\overline{u}^n_{j-1/2}$ and the two values $\delta u^n_j$ and $\delta u^n_{j-1}$. It can be seen as a *local model* at the scale of the box $K_{j-1/2}$. We use a model with 3 parameters consisting of a relaxation scheme in the form [5,7]

$$\begin{aligned}\left(\frac{1}{2} + D^n_{U,j-1/2}\right)\,\delta u^n_j + \left(\frac{1}{2} - D^n_{U,j-1/2}\right)\,\delta u^n_{j-1} - \delta\overline{u}^n_{j-1/2} = \\ -\frac{\zeta^n_{j-1/2}}{\delta t}\,(M^n_{E,j-1/2} - \overline{u}^n_{j-1/2}),\end{aligned} \tag{4.5}$$

where $M^n_{E,j-1/2}(u)$ stands for an *equilibrium average value* defined by

$$M^n_{E,j-1/2}(u) = \left(\frac{1}{2} + D^n_{E,j-1/2}\right)\,u^n_j + \left(\frac{1}{2} - D^n_{E,j-1/2}\right)\,u^n_{j-1}. \tag{4.6}$$

Finally, we need a local model for (4.2) expressing the closure law for the diffusive flux $p$. We use an upwinded quadrature formula in the form

$$\bar{p}_{j-1/2}(t) = \frac{1}{2}\,[p_j(t) + p_{j-1}(t)] - D_{p,j-1/2}(t)\,[p_j(t) - p_{j-1}(t)]. \tag{4.7}$$

Equations (4.5) and (4.7) contain 4 parameters in each box $K_{j-1/2}$ at each time $t^n$, which have to be specified: the two upwind parameters, $D_{U,j-1/2}$ and $D_{E,j-1/2}$, arising in (4.5) and (4.6), respectively; a time parameter $\zeta_{j-1/2}$ for defining the relaxation time scale $\delta t/\zeta_{j-1/2}$ in (4.5); and the parameter $D_{p,j-1/2}$ for the definition of the average of the diffusive flux $p$ in (4.7).

The values taken by the four above parameters relies on the numerical analysis presented in [6,7]. It consists, on the one hand, of a time-independent analysis, allowing to select $D_p$ in a way ensuring a non-oscillating stationary state for the convection-diffusion equation [6]; on the other hand, of a time-dependent analysis based on the notion of *equivalent equation* [7]. This allows to define the three parameters $D_U$, $D_E$, and $\zeta$ to achieve a high-order accuracy. Note that the present box-scheme can be expressed as a 3-point implicit scheme in the incremental values $\delta u^n_j$. Finally, we stress the fact that the box-scheme is used in both the parabolic and the hyperbolic subdomains. It has been proved to be accurate in all Peclet regimes.

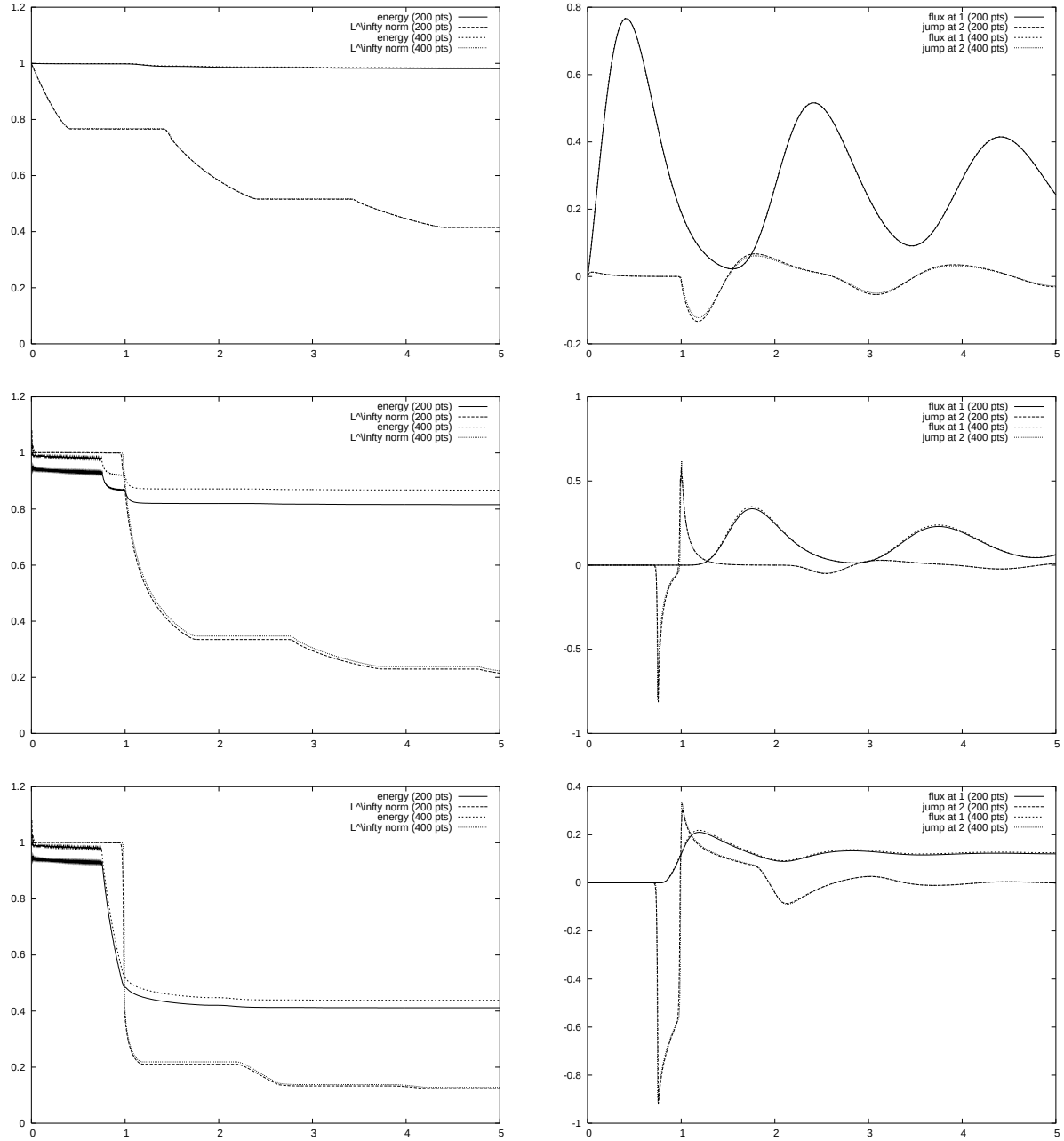


**Figure 6.** Numerical results obtained with the box-scheme: case 1 (top), case 2 (center), and case 3 (bottom). Left panels: normalized energy and $L^\infty(\Omega)$-norm of the solution; right panels: the flux at $x = 1$ and the jump at $x = 2$.

Results with equispaced meshes of 200 and 400 boxes are displayed on Fig 6. In all computations, the time step is selected according to a CFL number of $\frac{\delta t}{h} = 0.5$. We consider the time evolution of the normalized energy, the $L^\infty$ norm of the solution, the flux at $x = 1$, and the jump at $x = 2$. The accuracy of the scheme can be observed on the low energy dissipation and on the sharp resolution for the jump at $x = 2$. For instance, at time $t = 5$ and for case 2, the value of the energy is underestimated by 7.6% on the coarse grid and by 1.7% on the fine grid, a significant improvement with respect to the upwind scheme.

### 4.3. Local Discontinuous Galerkin (LDG)

The local discontinuous Galerkin method was developed by Cockburn and Shu [3] for convection-diffusion equations based on earlier work devoted to hyperbolic conservation laws. A complete review of the LDG method and other discontinuous Galerkin methods can be found in [4] and references therein.

Let $\mathscr{M} = \cup_{j=1}^{N}[x_j, x_{j+1}]$ be a mesh of $\Omega$. As for the finite volume box scheme, we assume that the mesh is compatible with the partitioning of $\Omega$ into $\Omega_P$ and $\Omega_H$, i.e. that a mesh node is located at point $x = 1$. Let $k \geqslant 1$ be an integer. Let $V^{\mathrm{DG}}$ be the space of piecewise discontinuous functions in $\Omega$ that are polynomials of degree $\leqslant k$ in each mesh cell $[x_j, x_{j+1}]$ for $1 \leqslant j \leqslant N$. Let $V_P^{\mathrm{DG}}$ be the subspace of $V^{\mathrm{DG}}$ spanned by those functions that vanish identically on $\Omega_H$. For a function $v_h \in V^{\mathrm{DG}}$, we denote its trace at a point $x_j$ in the mesh as

$$v_h^{\pm}(x_j) = \lim_{s \to 0^+} v_h(x_j \pm s), \quad 1 \leqslant j \leqslant N, \tag{4.8}$$

and we define its jump and average across inner element boundaries as

$$[v_h(x_j)] = v_h^+(x_j) - v_h^-(x_j) \quad \text{and} \quad \{v_h(x_j)\} = \tfrac{1}{2}(v_h^+(x_j) + v_h^-(x_j)), \quad 1 \leqslant j \leqslant N.$$

The LDG method consists of seeking $u_h \in C^1([0,\infty[; V^{\mathrm{DG}})$ such that $\forall v_h \in V^{\mathrm{DG}}$ and $\forall t \geqslant 0$,

$$\begin{aligned} \frac{\mathrm{d}}{\mathrm{d}t}(u_h, v_h)_\Omega - (u_h + z_h, v_{h,x})_\Omega - \sum_{x_j \in \Omega} u_h^-(x_j)\,[v_h(x_j)] \\ - \sum_{x_j \in \Omega_P} \{z_h(x_j)\}[v_h(x_j)] - z_h^-(1)[v_h(1)] = (f, v_h)_\Omega, \end{aligned} \tag{4.9}$$

and $z_h \in C^0([0,\infty[; V_P^{\mathrm{DG}})$ such that $\forall v_h \in V_P^{\mathrm{DG}}$ and $\forall t \geqslant 0$,

$$\begin{aligned} (z_h, w_h)_\Omega - \alpha_0 (u_h, w_{h,x})_\Omega - \sum_{x_j \in \Omega_P} \alpha_0 \{u_h(x_j)\}\, w_h[(x_j)] \\ + \alpha_0 \left( (u_h w_h)(1^-) - (u_h w_h)(0^+) \right) = 0. \end{aligned} \tag{4.10}$$

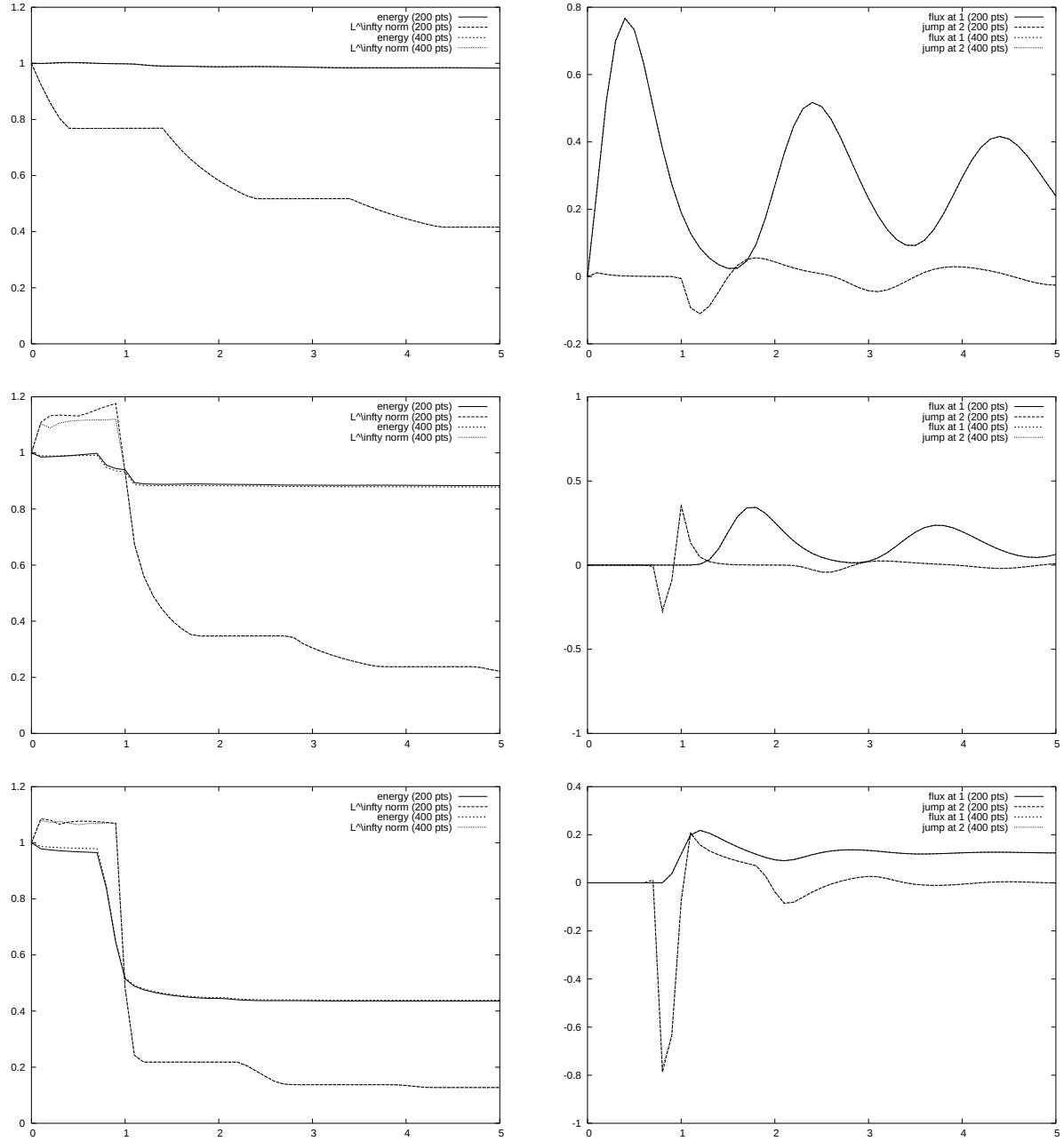


**Figure 7.** Numerical results obtained with the LDG method: case 1 (top), case 2 (center), and case 3 (bottom). Left panels: normalized energy and $L^\infty(\Omega)$-norm of the solution; right panels: the flux at $x = 1$ and the jump at $x = 2$.

Note that (4.10) is a local reconstruction formula for the diffusive flux $\zeta_h = -\alpha_0 u_{h,x}$ in $\Omega_P$, while (4.9) is the discretization of the evolution equation using the reconstructed flux. As for the finite volume box scheme, the continuity of the solution at point $x = 1$ is not used. Furthermore, the periodicity of the flux is weakly enforced in (4.9). Finally, Problem (4.9)–(4.10) is discretized in time via a simple explicit Euler method (without slope limiting).

Numerical results are presented in Figure 7. Two uniform meshes of $\Omega$ are considered: a coarse mesh with 200 cells and a fine mesh with 400 cells. The time step is obtained from the diffusive stabilty limit $\delta t = \frac{1}{10}\frac{h^2}{\alpha_0}$. As before, we show the time evolution of the normalized energy, the $L^\infty(\Omega)$-norm of the solution, the flux at $x = 1$, and the jump at $x = 2$ estimated by the difference $u(t,2) - u(t,2-h)$; see the two upper panels of Figures 2–4 for a comparison with the reference solution. For case 1 where the initial data is smooth, excellent agreement is obtained. For cases 2 and 3 where the initial data is rough, the Gibbs phenomenon is triggered causing the $L^\infty(\Omega)$-norm of the solution to be larger than one until the wave has entered completely the parabolic subdomain. It is well-known that this phenomenon can be cured by the use of a suitable slope limiter, but this is not the scope of the present work. We also observe that the jump at point $x = 2$ is captured with little accuracy. At time $t = 5$ and for case 2, the value of the energy is underestimated by 2.9% on the coarse grid and by 1.2% on the fine grid, yielding a level of accuracy comparable to that of the box-scheme.

## 5. CONCLUDING REMARKS

In this paper, we have analyzed a degenerate one-dimensional advection-diffusion equation with periodic interface conditions for the total advective-diffusive flux. Using the evolution linear semi-groups theory, we have shown that the associated Cauchy problem is well-posed provided an additional continuity condition is enforced on the solution at the parabolic to hyperbolic interface. Reference solutions have been obtained for various sets of data (initial condition, diffusion coefficient) and can now be used by practitioners to test the robustness of numerical schemes to approximate flows in media with strong heterogeneities.

To conclude, we point out that various interesting theoretical points have been postponed to future work. A classical question to which it is often difficult to answer is to know in which sense the function $u(t) = T(t)u_0$ given by the semi-group theory solves the evolution problem when the initial condition is too rough to be in the domain of the evolution operator. Although we have constructed a weak solution to the evolution problem for a rather general class of initial conditions, it is not yet clear that these solutions are those given by the semi-group theory. Furthermore, another viewpoint worth pursuing to analyze the evolution problem is that of periodic distributions by seeking the Fourier series of the solution. Finally, it would be interesting to perform a convergence analysis of the various schemes presented above.

**Acknowledgments.** The authors are grateful to E. Cancès, R. Eymard, and R. Monneau for various fruitful discussions.

## REFERENCES

1. H. Brezis, *Analyse fonctionnelle*. Masson, Paris, 1987.
2. T. Cazenave and A. Haraux, *Introduction aux problèmes d'évolution semi-linéaires*. Ellipses, Paris, 1990.
3. B. Cockburn and C.-W. Shu, The local discontinuous Galerkin method for time-dependent convection-diffusion systems, *SIAM J. Numer. Anal.* (1998) **35**, 2440–2463.
4. B. Cockburn, G. Karniadakis, and C. Shu, The development of discontinuous Galerkin methods. In *Discontinuous Galerkin Methods* (Eds. B.Cockburn, G.Karniadakis, and C.Shu). Springer-Verlag, Berlin, 2000.
5. B. Courbet, Etude d'une famille de schémas boˆite à deux points et application à la dynamique des gaz monodimensionnelle. *La Recherche Aérospatiale* (1991) **5**, 31-44.
6. J-P. Croisille, Keller's box-scheme for the one-dimensional stationary convection-diffusion equation. *Computing* (2002) **68**, 37–63.
7. J-P. Croisille, A high order accurate box-scheme for the one dimensional convection-diffusion equation. Preprint, Metz University (2002).
8. J.-P. Croisille and I. Greff, An efficient box-scheme for convection-diffusion equations with sharp contrasts in the diffusion coefficient. Preprint, Metz University (2002) submitted.
9. F. Gastaldi and A. Quarteroni, On the coupling of hyperbolic and parabolic systems: Analytical and numerical approach. *Appl. Num. Math.* (1989) **6**, 3–31.
10. F.M. Holly and A. Preissmann, Accurate calculation of the transport in two dimensions. *Journal of Hydraulics division* (1977) 1259–1277.
11. J.-L. Lions, *Quelques méthodes de résolution des problèmes aux limites non linéaires*. Dunod, Paris, 1969.
12. A. Pazy, *Semigroups of Linear Operators and Applications to Partial Differential Equations*. Springer, New York, 1983.
13. A. Quarteroni and A. Valli, *Numerical Approximation of Partial Differential Equations*. Springer, Berlin, 1997.